Tuning magnetic hysteresis of electrodeposited Fe 3 O 4

Shawn Chatman, Adam J. G. Noel, and Kristin M. Poduska

Citation: Journal of Applied Physics **98**, 113902 (2005); doi: 10.1063/1.2135892
View online: http://dx.doi.org/10.1063/1.2135892
View Table of Contents: http://scitation.aip.org/content/aip/journal/jap/98/11?ver=pdfcov
Published by the AIP Publishing

Tuning magnetic hysteresis of electrodeposited Fe_3O_4

Shawn Chatman, Adam J. G. Noel, and Kristin M. Poduska[a)]
Department of Physics and Physical Oceanography, Memorial University of Newfoundland, St. John's, Newfoundland, A1B 3X7, Canada

(Received 24 February 2005; accepted 17 October 2005; published online 2 December 2005)

We demonstrate that changes in electrolyte composition and applied potential during aqueous electrodeposition can be used to tune the magnetic hysteresis response of thin-film Fe_3O_4 (magnetite) on polycrystalline metal substrates. X-ray diffraction data confirmed that magnetite formation in electrolytes containing KCH_3COO (0.04–2.0 *M*) and $Fe(SO_4)_2(NH_4)_2$ (0.01*M*) required temperatures between 60 and 85 °C, and deposition potentials between −0.300 and −0.575 V or galvanostatic current densities between 50 and 88 $\mu A/cm^2$. Scanning electron microscopy studies show that magnetite crystallites tend to adopt different habits depending on the electrolyte composition. Room-temperature magnetic hysteresis responses (squareness and coercivity) are dependent upon the crystal habit of deposits, implying that the electrolyte's acetate concentration influences the magnetic domain structure of the resulting magnetite deposits. Magnetite crystallites grown from electrolytes with low acetate concentrations showed pseudo-single-domain magnetic response, while magnetite grown from acetate-enriched electrolytes showed multidomain magnetic response. © *2005 American Institute of Physics*.
[DOI: 10.1063/1.2135892]

I. INTRODUCTION

Magnetite (Fe_3O_4), historically known as lodestone, has become the focus of renewed technological interest in magnetic and electronic applications. In magnetite (space-group $Fd\bar{3}m$), close-packed oxygen layers accommodate Fe^{3+} ions in tetrahedral sites, while the octahedral sites contain an equal mixture of Fe^{2+} ions and Fe^{3+} ions.[1] The exchange integrals within and between these sublattices favor an antiparallel spin alignment. However, the interaction between the sublattices is dominant, yielding parallel alignment within each sublattice, but an antiparallel alignment between them. The result is a net ferrimagnetic moment from the Fe^{2+} ions. The competition between spins on the two Fe sublattices also results in unusual, half-metallic electronic properties for magnetite. Magnetite is reported to be 100% spin polarized at the Fermi energy,[2,3] and its potential in spintronic devices has been a topic of recent research interest.[4–6]

For any magnetic device application, material microstructure is a crucial characteristic. Grain size and crystallite orientations play an important role in magnetic properties such as hysteresis and remanent magnetization, as well as magnetoresistance.[7] These microstructural features, in turn, are determined by the conditions under which the material was prepared and treated. Therefore, controlling synthesis conditions is of critical importance for developing reliable functional magnetic materials.

Traditionally, thin films of magnetite have been synthesized using techniques such as molecular beam epitaxy,[8] electron beam evaporation,[9] and laser ablation.[10] These methods involve ultrahigh vacuum (UHV) synthesis as well as deposition and/or annealing treatments at high temperatures, both of which increase the cost of production. Such methods are also incompatible with substrates which degrade at relatively low temperatures, such as GaAs.[10,11] Electrodeposition is an economical, lower-temperature alternative, and has been applied to iron oxide materials.[12–14] Evidence from the literature suggests that, in general, changes in deposition potential and electrolyte composition can have dramatic effects on film formation, including crystallinity, grain size, and orientation.[15–17] This points to a need for studies which address how the quality of magnetite electrodeposits varies with deposition potential, as well as the electrolyte *p*H and composition.

Addressing this need, we have explored the relationship between synthesis conditions of magnetite and the resulting structural, microstructural, and magnetic characteristics. We interpret changes in the magnetic hysteresis behavior in terms of synthesis-induced tuning of the magnetic domains.

II. EXPERIMENTAL SECTION

A. Sample preparation

We prepared thin films of iron oxide materials by modifying a procedure reported by Sorenson *et al.*,[5] based on the earlier studies of Nishimura *et al.*,[12] involving a net cathodic (reducing) current.

$$2FeOH^{2+} + FeOH^{+} + OH^{-} \rightarrow (Fe^{3+},Fe^{2+})_3O_4 + 4H^{+}. \quad (1)$$

This reaction is not a simple reduction-oxidation reaction, but rather is a series of reactions assisted by anodic oxidation of Fe^{2+} to Fe^{3+}. The aqueous electrolyte contained an iron (II) salt, 0.01 *M* $Fe(SO_4)_2(NH_4)_2 \cdot 6H_2O$, as well as a complexing agent KCH_3COO, which also introduces a slight buffering effect. Electrolyte *p*H increased with the concentration of potassium acetate, ranging from *p*H=6.0 (at 0.04 *M*) to 8.5 (at 2.0 *M*). Most depositions in this study

[a)]Electronic mail: kris@physics.mun.ca; URL: http://www.physics.mun.ca/~kris/

involved the more acidic electrolyte containing 0.04 *M* KCH_3COO, so this is the concentration used unless otherwise noted. Supplementary studies involved 0.1 *M* NH_4CH_3COO in place of potassium acetate, resulting in an electrolyte *p*H of 6.7. All electrolytes were prepared from ACS grade reagent salts (EM Scientific) and ultrapure water (Barnstead Nanopure, 18.2 MΩ cm).

Films were deposited either with a constant applied potential (−0.300 to −0.450 V) or under constant current conditions (50 or 88 $\mu A/cm^2$) in a standard three-electrode cell using a Hokuto Denko HA 501 potentiostat/galvanostat. These potential and current density ranges include conditions described in previous magnetite electrodeposition experiments.[5,13] Our investigations spanned the useful potential limits for magnetite nucleation and growth in the electrolytes described above. The data were recorded and analyzed using LABVIEW (National Instruments) user interfaces of our own design. Working electrodes were polycrystalline brass disks (shimstock) or (111)-textured evaporated Au/Cr/glass (Erie Scientific). Au/Cr/glass slides were stored immersed in concentrated H_2SO_4, while the brass electrodes were dipped in concentrated HCl immediately prior to use. A gold wire served as a counter electrode, and all potentials in this work are quoted with respect to a Ag/AgCl reference electrode (Fisher Scientific). Electrolyte temperatures above 70 °C were required for deposition, and deposits for this study were typically prepared in 10–90 min at 80 °C. At temperatures above 85 °C, vaporization of the electrolyte created problematic bubbles on the working electrode. A thorough argon purge prior to and during deposition removed O_2 from the solution and suppressed the formation of iron hydroxide precipitates. After deposition, the samples were rinsed with ultrapure water and then dried in argon gas to reduce subsequent formation of undesired surface iron oxide and hydroxide species. Sample masses were measured using an analytical balance, and then converted to effective thicknesses using the density of magnetite (5.21 g/cm^3) and deposit area (typically 0.4 cm^2). Sample thicknesses were typically 50–200 nm after 15–45 min of deposition, corresponding to current efficiencies near 75%.

Visual inspection of the samples was carried out immediately after deposition. Films indicative of magnetite were typically smooth, black, and adhered well to the substrate. Color is a simple, yet important, identifier in phase determination. Bulk magnetite shares its black color with another closely related iron oxide phase, maghemite (γ-Fe_2O_3). On the other hand, red deposits are indicative of hematite (α-Fe_2O_3) or iron hydroxides such as goethite (γ-FeOOH). Therefore, the deposited black films merited further analysis to accurately determine their phase compositions.

B. XRD analysis

X-ray diffraction (XRD) data were obtained with a Debye-Scherrer powder diffractometer (Rigaku D/MAX 2200PC), in the θ-θ geometry, using Cu $K\alpha$ radiation. Scan parameters were typically 15–100° 2θ, at a rate of 0.5°/min with a step size of 0.05° 2θ. Linear least-squares lattice-constant refinements were facilitated with the LATCON software package.[18]

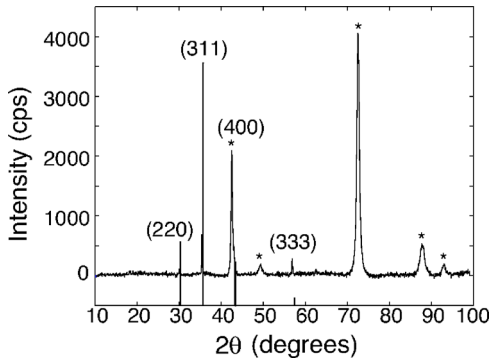

FIG. 1. Indexed XRD pattern from a thin film (~100 nm thickness) of magnetite prepared by potentiostatic deposition at −0.375 V. Peaks resulting from the brass substrate are marked with an asterisk (*). The observed Bragg reflections are excellent matches with those expected for magnetite, JCPDS #19-0629.

C. Scanning electron microscopy

A scanning electron microscope (SEM) (Hitachi S570) with attached energy dispersive X-ray (EDX) spectrometer (Tracor Northern EDX) provided morphological and qualitative compositional information on the deposits. Samples were gold coated prior to SEM analysis to improve resolution at high magnification. The EDX spectrometer was capable of identifying atoms with atomic masses greater than neon.

D. Magnetometry

Magnetic data were acquired with a Quantum Designs MPMS XL superconducting quantum interface device (SQUID) magnetometer at temperatures between 50 and 298 K, and in fields up to 0.1 T. Data were corrected for the net diamagnetic contributions from substrate and the gelatin capsule sample container.

III. RESULTS AND DISCUSSION

A. Structural variation with deposition potential

XRD studies confirm that electrodeposition of magnetite is possible over a rather small range of potentials. Black films deposited between −0.350 and −0.425 V were consistently single phase magnetite. As a demonstration of phase purity, Fig. 1 shows an XRD scan from an electrodeposited film prepared at −0.375 V. Lattice-constant refinements yield a cubic unit cell with lattice constant $a=8.396\pm0.009$ Å, which is in excellent agreement with that of magnetite (8.397 Å, JCPDS#19-0629).[19] Miller indices of the observed peaks are consistent with magnetite's $Fd\bar{3}m$ space-group assignment. To assess the degree of preferred orientation, peak intensities of deposits on both brass and Au/Cr/glass substrates were compared to those expected for a randomly ordered powder sample. These analyses suggest minimal preferred orientation, although overlaps between the magnetite and substrate peaks make a quantitative determination diffi-

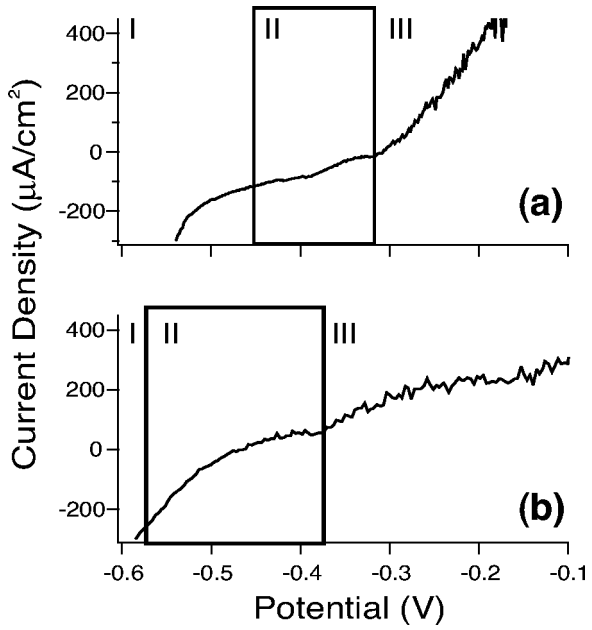

FIG. 2. Linear sweep voltammograms at 1 mV/s reveal features in the current vs applied potential profile for samples deposited using (a) 0.04 and (b) 1.0 *M* potassium acetate. Section I indicates the potential range where no deposits are formed, section II indicates the region where magnetite deposition occurs, and section III indicates the region where goethite forms.

cult. EDX analyses confirmed the presence of iron in all samples, and no evidence of other metals, aside from substrate elements, was present.

Black films synthesized at more positive potentials tended to yield a secondary phase. Careful analysis of lattice-constant refinements showed that samples deposited between −0.325 and −0.300 V were typically comprised of two cubic materials, with lattice constants $a=8.396\pm0.009$ Å and $a=8.360\pm0.009$ Å. These correlate with the cubic lattice constants of magnetite (8.397 Å) and maghemite (8.339 Å), respectively.[19] Since all Fe ions in maghemite are in a 3+ oxidation state, while magnetite has a mixture of Fe^{2+} and Fe^{3+} ions, it is reasonable to expect that the more oxidized material (maghemite) would form at more positive (oxidizing) deposition potentials.

Figure 2(a) indicates the limits of magnetite formation, as confirmed by XRD, for the electrolyte containing 0.04 *M* acetate. This positive (linear) sweep voltammogram, for a 1 mV/s sweep rate, spans the relevant region of applied potential (−0.550 to −0.100 V). The large cathodic current at potentials more negative than −0.540 V is a result of hydrogen evolution. Since visible deposits form only at applied potentials more positive than −0.425 V, hydrogen evolution does not compete or interfere with iron oxide formation. At potentials more positive than −0.300 V, reddish deposits characteristic of the iron oxide hydroxides γ-FeOOH (goethite) prevailed. This region of the voltammogram displays a substantially noisier current trace, which is consistent with the fact that both maghemite and goethite have a much lower electrical conductivity than magnetite. These potential limits for magnetite electrodeposition do not show any significant variation among deposits on either brass or gold substrates.

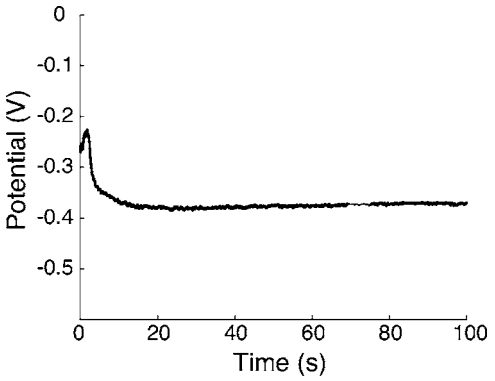

FIG. 3. Applied deposition potential vs time for a sample prepared galvanostatically at 50 μA/cm^2. Within the first 15 s of deposition, the applied potential stabilizes to a potential at which magnetite is electrodeposited, and no significant variation in potential is observed over 15–90 min of deposition.

However, these limits do shift with changes in electrolyte composition, as shown in Fig. 2(b) and discussed below.

Magnetite can also form under constant current (galvanostatic) deposition conditions. XRD data suggest that magnetite forms when current densities are between 50 and 88 μA/cm^2. Figure 3 highlights the fact that the applied voltage varies over time for a galvanostatic deposition at 50 μA/cm^2. After a short initial period (10–20 s) at more positive potentials, the applied potential stabilizes to a value at which magnetite forms.

Pourbaix diagrams, which are plots of calculated ion and solid-phase stabilities as a function of applied potential and *p*H, indicate that for the iron-water system at 25 °C, magnetite is stable from −0.500 to −0.300 V *vs* Ag/AgCl in *p*H ranges of 5.5–8.5.[20] Despite the higher temperatures and the complexing agents used in this work, the Pourbaix diagram calculations coincide well with the region of magnetite formation we report.

B. Microstructural characterization

SEM yielded information on deposit homogeneity, crystallite morphologies, and grain sizes in the iron oxide electrodeposits. At all potentials and current densities, angular octahedral crystallites were the dominant morphology, as shown in Fig. 4. This shape indicates the crystal growth that occurs more slowly along the ⟨111⟩ direction. For shorter deposition times, octahedral crystallites appear to grow separately, while with longer deposition times, larger polycrystal-

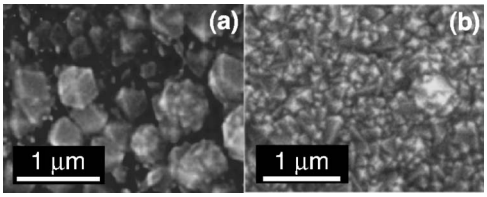

FIG. 4. Scanning electron micrographs show angular crystallites in deposits synthesized both galvanostatically (a), at 50 μA/cm^2, and potentiostatically (b), at −0.375 V.

line conglomerates tend to form. Deposit morphologies were typically quite consistent across the entire (7 mm diameter) sample.

By examining the broadening of XRD peaks, we were also able to determine a mean crystallite size using the Scherrer formula,

$$t = \frac{0.9\lambda}{B \cos \theta_B}, \tag{2}$$

wherein t is the crystallite size, λ is the radiation wavelength, B is the width of a diffraction peak at half maximum, and θ_B is half the 2θ value of said peak.[21] Using this kind of analysis, instrumental broadening could lead to an underestimation of crystallite sizes. However, the agreement between SEM micrographs and the calculated crystallites sizes ($\approx$50–150 nm) suggests that the instrumental broadening is not a significant factor in the observed peak widths.

Few other reports of electrodeposited magnetite films exist, and those that describe deposits on polycrystalline substrates do not comment extensively on crystallite size or habit. Zhang *et al.*[22] report the square grains in deposits prepared on polycrystalline substrates from electrolytes containing $FeSO_4$ and NH_4CH_3COO using 1 kHz alternating electric fields. Using a dc electric field in $FeCl_2$ and a *p*H-adjusting solution of ammonia, Nishimura *et al.*[12] also synthesized magnetite on polycrystalline substrates, observing changes in roughness depending on the ammonia concentration. More recent reports from Nikiforov *et al.*[13] demonstrate that high-quality epitaxial magnetite deposits form on low index planes of gold single crystals, including triangular crystallites on Au(111). Peulon *et al.*[14] have also observed octahedral crystallites of magnetite electrodeposited on polycrystalline gold substrates from electrolytes containing NaCl, $FeCl_2$, and 1-methyl-imidazole.

C. Effect of electrolyte composition

The concentration of ammonium ions in the electrolyte impacts magnetite formation. With a sixfold increase in the ammonium concentration, yielding a ratio of 0.12 *M* NH_4 to 0.01*M* Fe (*p*H=6.7), no magnetite deposits formed. Goethite (γ-FeOOH) formed at potentials more positive than −0.275 V while no deposit formed at more negative potentials. However, eliminating all ammonium from solution, using $FeSO_4 \cdot 7H_2O$ instead of $Fe(SO_4)_2(NH_4)_2 \cdot 6H_2O$ (electrolyte *p*H=6.97), was not detrimental to magnetite formation.

Since our findings do not appear to be related solely to changes in electrolyte *p*H, it is interesting to compare with other studies of magnetite deposition in the presence of ammonium ions. Nishimura *et al.* investigated the effect of ammonia concentrations on magnetite electrodeposition under potentiostatic conditions in a flow-through cell using $FeCl_2$ as the Fe^{2+} source and NH_3 as a *p*H-adjusting solution.[12] They report a maximum deposition rate for a NH_3 concentration of 14.8 *mM*, and they attribute the decrease in the deposition rate of magnetite at higher NH_3 concentrations to the onset of iron hydroxide precipitation at *p*H values greater than 6.9. In contrast, we do not observe precipitates, but rather the deposition of a different iron oxide phase for higher ammonium concentrations near 1.0 *M*.

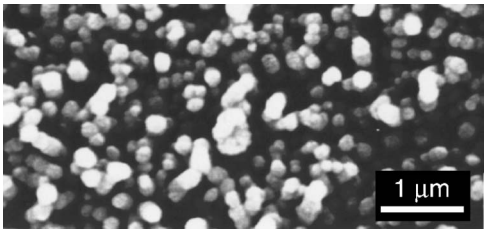

FIG. 5. Scanning electron micrographs show that rounded, columnar crystallites appear in deposits synthesized potentiostatically, in this case at −0.425 V, from electrolytes with higher acetate concentrations (1.0–2.0 *M*).

Acetate ion concentration also plays an important role in magnetite electrodeposition. Increasing the acetate concentration to 1.0*M* caused a shift in the deposition potential range to more negative values, shown in Fig. 2(b), as expected from the increased basicity of the electrolyte (*p*H =8.25). Additionally, the potential range over which black deposits formed expanded to −0.375 to −0.575 V. These deposits were visually comparable to those synthesized with 0.04 *M* acetate, but grew much faster. For example, a 10 min deposition with 1.0 *M* acetate yielded a similar thickness to a 30 min deposit with 0.04 *M* acetate (both ~100 nm thick), each prepared at an overpotential of 0.23 V, relative to the *p*H-dependent Nernst reversible potential for the oxidation of Fe^{2+} to Fe^{3+} (−0.63 V *vs* Ag/AgCl at 25 °C and 1 atm). A further increase in the acetate concentration to 2 *M* resulted in a small *p*H difference (*p*H=8.5), as well as a decreased potential window for magnetite deposition (0.425 to −0.525 V). Again, these deposits appeared similar to those from electrolytes with lower acetate concentrations, and grew at a rate comparable to those formed from electrolytes with 1 *M* acetate over the whole deposition potential range. Crystalline deposits containing a mixture of maghemite and magnetite were synthesized between −0.425 and −0.500 V.

Electrolytes with higher acetate (1.0–2.0 *M*) concentrations enable magnetite deposition at temperatures as low as 60 °C, but often with poorer crystallinity according to the XRD data. Additionally, different deposit morphologies appeared, including rounded columnar features, as shown in Fig. 5. With either 1.0 *M* or 2.0 *M* acetate, as with lower acetate concentrations, goethite formed readily at more positive potentials, while no deposits formed at more negative potentials.

D. Magnetic hysteresis

Figure 6 shows the representative hysteresis loops for electrodeposited magnetite, obtained at 298 K with a maximum applied field of 1000 Oe in the plane of the film. The most obvious differences among hysteresis loops are the magnitudes of the coercivities and loop squareness. There was no appreciable difference between the perpendicular and in-plane hysteresis loop data, either in the magnetic coercivity values or the saturation magnetizations. This suggests that our polycrystalline samples, with thicknesses in the 100 nm range, are bulklike and display no significant influence from

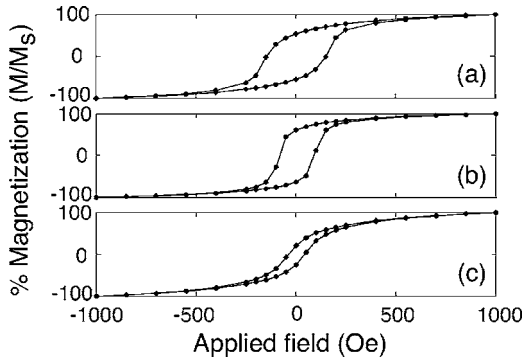

FIG. 6. Representative hysteresis loops obtained from potentiostatically deposited samples at −0.325 V (a), −0.350 V (b), and −0.425 V (c). The square loops in (a) and (b) are from the deposits prepared from electrolytes with 0.04 *M* acetate, while the round loop in (c) is from a deposit prepared from an electrolyte containing 2 *M* acetate.

the substrate. This is consistent with the fact that deposits did not exhibit substrate-dependent crystallite morphologies, crystallite orientations, or magnetic coercivities. The magnitude of the coercivities we report here are comparable to those reported by Zhang *et al.* for magnetite electrodeposited under alternating current conditions.[22]

Other aspects of the magnetic measurements show definitive characteristics of Fe_3O_4. A broad Verwey transition near 115 K was observed in the temperature-dependent magnetization, consistent with the previous studies of thin magnetite films prepared by other methods.[7] Additionally, saturation magnetization values for single-phase deposits are consistent with the theoretical value of 92 emu/g for bulk magnetite. Multiphase samples prepared at more positive potentials exhibited consistently lower magnetization per mass, as would be expected because the secondary phases, such as γ-FeOOH and γ-Fe_2O_3, have a volume magnetization that is lower than that of magnetite.

Our magnetic coercivity data, shown in Fig. 7, suggest a strong correlation between more positive deposition potentials and larger coercivities. To compare deposits prepared from electrolytes with different *p*H values, we express all deposition potentials as overpotentials relative to the

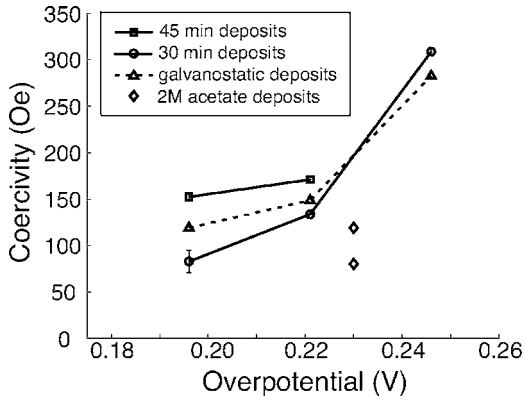

FIG. 7. Magnetic coercivity plotted as a function of overpotential shows a strong trend of increasing coercivity with increasing underpotential. All coercivity data were obtained with a field applied in the in-plane orientation. The overpotentials are calculated relative to the *p*H-dependent Nernst reversible potential for oxidation of Fe(II) to Fe(III).

*p*H-dependent Nernst reversible potential for the oxidation of Fe^{2+} to Fe^{3+}. Empirically, this *p*H dependence translates into a shift of +59 mV with each decreasing *p*H unit.

It is interesting to note that deposits prepared from electrolytes with high (1.0–2.0 *M*) acetate concentrations, and thus more basic *p*H values, exhibit coercivity values comparable to those from electrolytes with lower acetate concentrations. The primary difference in the magnetic response of such deposits is that their hysteresis loops are substantially less square than those prepared with 0.04 *M* acetate. As shown in Fig. 6(c), the remanent magnetization for these deposits is typically $<0.4\ M_s$, and the saturation magnetization is greater than 1000 Oe.

Preliminary direct investigations of domain structure in our electrodeposited magnetite crystallites using magnetic force microscopy (Asylum Research MFP-3D with CoCr-coated Si cantilevers) have proven difficult due to abrupt and dramatic height variations between the large polycrystallites and the smaller single crystallites. While evidence of multiple domains in larger crystallites was apparent from these initial investigations, further studies would benefit from a more uniform distribution of crystallite sizes.

IV. CONCLUSIONS

Given the dramatic difference in crystallite shape between the low and high acetate deposits, it is not surprising to see different magnetic responses. Coercivity is strongly affected by grain size and shape, as it is governed by how readily domains can reorient (or how readily domain walls can move) in the presence of an applied magnetic field. For magnetite, crystallites below 80 nm in size are typically comprised of a single magnetic domain, showing large coercivities and large remanent magnetizations, while larger crystallites tend to accommodate multiple domains, yielding smaller coercivities and smaller remanent magnetizations.[23] The magnetite deposits in this study, however, show small coercivities but large remanent magnetizations, which puts them in the category of pseudo-single-domain materials. This behavior is typically observed in magnetite with crystallite sizes ranging from 100 nm to 20 μm,[23] as they are in our deposits. This pseudo-single-domain classification is also reasonable given that SEM images from low acetate deposits show evidence of both larger polycrystallites (typically 500–1000 nm in diameter) and smaller single crystallites in our magnetite deposits (typically 50–150 nm in diameter). The rounded, columnar deposits from electrolytes with high acetate concentrations were less crystalline, according to XRD data, and exhibited more rounded hysteresis loops typical of samples containing multidomain crystallites. Since crystallite sizes were comparable to those in deposits from low acetate electrolytes (both ~100 nm), it appears that crystallite size alone does not determine the magnetic domain structure of our magnetite crystallites. Instead, our results show that varying the concentration of acetate in the electrolyte can be used to create either multidomain or pseudo-single-domain magnetite crystallites. This has implications for using electrodeposited Fe_3O_4 thin films for magnetic or magnetoresistive device applications.

ACKNOWLEDGMENTS

We thank Y.-H. Lee (SEM), Dr. M. Lemaire and Professor L. Thompson (SQUID), and Professor J. Shirokoff (XRD) for instrument facilities at Memorial University of Newfoundland. Additional thanks to Dr. R. Proksch (Asylum Research) for assistance with MFM measurements. We also gratefully acknowledge financial support from the Natural Science and Engineering Resource Council (Canada), Canada Foundation for Innovation New Opportunities Fund, and Memorial University of Newfoundland.

[1]E. J. W. Verwey, Nature (London) **144**, 327 (1939).
[2]Z. Zhang and S. Satpathy, Phys. Rev. B **44**, 13319 (1991).
[3]V. I. Anisimov, I. S. Elfimov, N. Hamada, and K. Terakura, Phys. Rev. B **54**, 4387 (1996).
[4]S. A. Wolf, D. D. Awschalom, R. A. Buhrman, J. M. Daughton, S. von Molnár, M. L. Roukes, A. Y. Chtchelkanova, and D. M. Treger, Science **294**, 1488 (2001).
[5]T. A. Sorenson, S. A. Morton, G. D. Waddill, and J. A. Switzer, J. Am. Chem. Soc. **124**, 7604 (2002).
[6]G. Hu and Y. Suzuki, Phys. Rev. Lett. **89**, 276601 (2002).
[7]M. Ziese and H. Blythe, J. Phys.: Condens. Matter **12**, 13 (2000).
[8]D. T. Margulies, F. T. Parker, M. L. Rudee, F. E. Spada, J. N. Chapman, P. R. Aitchison, and A. E. Berkowitz, Phys. Rev. Lett. **79**, 5162 (1997).
[9]Yu. S. Dedkov, M. Fonin, D. V. Vyalikh, J. O. Hauch, S. L. Molodtsov, U. Rüdiger, and G. Güntherodt, Phys. Rev. B **70**, 073405 (2004).
[10]R. J. Kennedy and P. A. Stampe, J. Phys. D **32**, 16 (1999).
[11]M. Abe, T. Itoh, Q. Zhang, and S. Kurozumi, IEEE Trans. Magn. **32**, 4183 (1996).
[12]K. Nishimura, Y. Kitamoto, and M. Abe, IEEE Trans. Magn. **35**, 3043 (1999).
[13]M. P. Nikiforov, A. A. Vertegel, M. G. Shumsky, and J. A. Switzer, Adv. Mater. (Weinheim, Ger.) **12**, 1351 (2000).
[14]S. Peulon, H. Antony, L. Legrand, and A. Chausse, Electrochim. Acta **29**, 2891 (2004).
[15]S. Peulon and D. Lincot, J. Electrochem. Soc. **145**, 864 (1998).
[16]M. Datta and D. Landolt, Electrochim. Acta **45**, 2535 (2000).
[17]R. M. Penner, J. Phys. Chem. B **106**, 3339 (2002).
[18]D. Schwarzenbach, LATCON. Program for the LS-refinement of Lattice Constants (Uni Lausanne, Switzerland, 1975).
[19]Joint Commission on Powder Diffraction Standards, Powder Diffraction File No. 19-0629 (International Centre for Diffraction Data, Newtown Square, PA, USA, 2003); URL: www.icdd.com.
[20]M. Pourbaix, *Atlas of Electrochemical Equilibria in Aqueous Solutions* (Pergamon, New York, 1966).
[21]B. D. Cullity and S. R. Stock, *Elements of X-Ray Diffraction* (Prentice-Hall, Upper Saddle River, 2001).
[22]Q. Zhang, T. Itoh, and M. Abe, IEEE Trans. Magn. **30**, 4900 (1994).
[23]D. J. Dunlop, J. Geophys. Res., [Solid Earth] **100**, 2161 (1995).